Role of domain walls in the abnormal photovoltaic effect in $BiFeO_3$

Akash Bhatnagar[1], Ayan Roy Chaudhuri [2], Young Heon Kim[3], Dietrich Hesse[1], and Marin Alexe[1,4*]

[1]Max Planck Institute of Microstructure Physics, D-06120 Halle, Germany

[2]Institute of Electronic Materials and Devices, Leibniz University, D-30167 Hannover, Germany

[3] Korea Research Institute of Standards and Science, Daejeon 305-304, Rep. of Korea

[4] University of Warwick, Department of Physics, Coventry CV8 2EN, United Kingdom

Abstract

Recently the anomalous photovoltaic effect in $BiFeO_3$ thin films, which resulted in open circuit voltages (V_{oc}) considerably larger than the band gap of the material, has generated a revival of the entire field of photoferroelectrics. In the present work, *via* temperature dependent photovoltaic studies we prove that the bulk photovoltaic effect, which has been studied in the past for many non-centro-symmetric materials, is at the origin of the anomalous photovoltaic effect in $BiFeO_3$ films. Moreover, we show that irrespective of the measurement geometry, V_{oc} as high as 50 V can be achieved by controlling the conductivity of domain walls. We also show that photoconductivity of the domain walls is markedly higher than in the bulk of $BiFeO_3$.

*Corresponding author: malexe@mpi-halle.mpg.de, M.Alexe@warwick.ac.uk

Recently the entire field of photoferroelectrics has been revitalized by reports of an abnormal photovoltaic (PV) effect in $BiFeO_3$ (BFO) thin films.[1] The main characteristics of this abnormal PV effect are very large open circuit photovoltages (V_{oc}) exceeding the band gap of the material. For instance, in high quality BFO thin films V_{oc} is several times larger than the band gap (~2.7 eV). However, reports on the photovoltaic effect in different BFO systems are rather contradictory. In a specific in-plane geometry of measuring electrodes with respect to the domain pattern, films with periodic ferroelectric/ferroelastic stripe domain patterns show V_{oc} values above[1] or below the band gap.[2] In the normal plane-parallel capacitor geometry the measured V_{oc} value has always been below the band gap values.[3,4] Single crystals show, or do not show, large V_{OC} values depending on the source or perhaps the crystal growth details.[5,6,7] To the best of our knowledge there is not yet any report of abnormal PV effect in BFO ceramics.

In the original report on the abnormal PV effect on epitaxial BFO films it was shown that V_{oc} values as large as 15 V can be obtained, but only in a specific geometry when the ferroelectric/ferroelastic domain walls are running parallel to the macroscopic electrodes. If the ferroelectric domains are perpendicular to the electrodes, there was no sizable PV effect, but only a photoconductive effect was detected.[1] This has led to the hypothesis that the abnormal PV effect in BFO originates solely in the domain walls by the following mechanism: The photo-generated electron-hole pairs (ehp) within the domain wall are separated by the strong field existing in this region, whereas within the bulk of the domains the carriers will strongly recombine. The separated electrons and holes will accumulate only at the domain walls (DW), building in such a way a small voltage across each domain wall. These voltages, although in the mV range, will sum up over macroscopic distances leading to the large open circuit voltage.[8] The bulk photovoltaic (BPV) effect which is known to exist in materials

lacking inversion symmetry such as $LiNbO_3$, $BaTiO_3$ or $Pb(Zr,Ti)O_3$,[9,10,11,12,13,14] was *a-priori* ruled out.

Subsequent experiments have shown that generation and recombination of photo generated carriers in BFO single crystals are primarily affected by the presence of shallow energy levels, and that domain walls are not playing a major role in the corresponding PV effect. Moreover, the photo-excited carriers are generated across the entire crystal and the recombination of these carriers is rather uniform and it is not necessarily stronger within the domains compared to the vicinity of the domain walls.[5,15]

We show here that the abnormal photovoltaic effect in BFO thin films with open circuit voltages as large as 50 V exists irrespective of the domain wall geometry and that the domain walls are playing a rather different role than initially proposed. We confirm that the abnormal PV effect in BFO is due to the bulk photovoltaic effect, as recently predicted by *ab-initio* calculations using the "shift currents" concept which have been able to predict the short-circuit photocurrent, *viz.* magnitude and even spectral features, demonstrating that these shift currents should dominate the bulk photovoltaic response in BFO.[16, 17]

Results

Thin film fabrication

Nominally 100 nm thick (001)-oriented $BiFeO_3$ epitaxial films were deposited by pulsed laser deposition on (110)-oriented $TbScO_3$ (TSO). Details on film growth and structure are given in the Methods section and Supplementary online material (SOM) (Supplementary Figure S1-S3). Samples showing stripe domains comprising either 109° or 71° domain boundaries have been fabricated by choosing the growth conditions. In case of 109° domains the stripes run along $[-110]_o$ whereas in 71° domains, stripes run along the $[001]_o$ direction. Figure 1 shows the corresponding piezo force microscope (PFM) images of the stripe domain

pattern obtained on the thin films with 71° domains and a cross-sectional TEM image of a sample with dominant 109° domains.

Platinum electrodes of 250 µm length and variable inter-electrode distances (from 15 µm up to 100 µm) were fabricated by sputter deposition using conventional photolithography and lift-off technique. Devices were aligned parallel and perpendicular to the domain walls, as shown schematically in Fig. 2 (also Supplementary Figure S4). The photoelectric effect was measured by illuminating the gap between the electrodes with a 405 nm ($h\upsilon$= 3.06 eV) laser with a maximum power of 80 mW and simultaneously measuring the photocurrent using a high-input impedance electrometer.

Abnormal photovoltaic effect

In order to get a better insight into the actual mechanism of the abnormal PV effect in BFO we have performed detailed photoelectric investigations on BFO epitaxial thin films with periodical domain patterns of 109° and 71° domain walls (DW), respectively. At room temperature (RT) both geometries, parallel to the domain walls (PLDW) and perpendicular to the domain walls (PPDW), show photovoltaic behavior similar to previous reports for 109° DW.[2] Current-voltage (IV) characteristics under illumination shown in Fig. 3 reveal V_{oc} values larger than the band gap of BFO (5 V for an inter-electrode gap of 100 µm) in the PLDW geometry and nearly zero for the DW running perpendicular to the electrodes. Surprisingly, the BFO sample comprising 71° DW shows at RT a sizable V_{oc} in both configurations, *viz.* -6.6 V perpendicular to the domain walls (PPDW) and -7.6 V parallel to the domain walls (PLDW), as shown in Fig. 3b.

Temperature dependent V_{OC}

Photoelectric measurements were conducted at temperatures ranging from 80K to 450K. By performing the analysis at different temperatures down to 80K we notice that in both geometries and DW variants by decreasing the temperature well below room temperature the V_{oc} values increase dramatically, i.e. for 109° domains to more than 17 V and for 71° domains to more than 50 V, as shown in Fig. 4. The temperature dependence of V_{oc} has a similar behavior for both geometries; it increases at low temperature to values which are in both cases well above the band gap with an obvious increase at temperatures lower than 200K. The most dramatic increase of V_{oc} to about 20 times the bang gap is for 71° DW. For 109° domains in the PPDW geometry the open circuit voltage which at RT was almost zero, becomes at 83K as large as 12 V. At RT in the case of 71° domains in the PPDW geometry, where according to the initial model the open circuit voltage should be below the band gap, the V_{oc} values are larger than 5V. The sizable V_{oc} in the perpendicular geometry in the case of 71° domains at RT and the dramatic increase of V_{oc} with decreasing temperature in all cases suggests that those mechanisms in which the domain walls are at the origin of this effect, as it has been previously assumed,[1,8] are not valid and both bulk and domain walls should play a different role.

Bulk photovoltaic effect

Keeping in perspective the temperature dependent behavior of V_{oc}, the only viable alternative explanation for the anomalous PV effect in BFO remains the bulk photovoltaic or photogalvanic effect, as known for materials lacking inversion symmetry, discovered by Chynoweth[9] and later analyzed theoretically by others[18,19]. Accordingly, under uniform illumination the photocurrent J_{ph} is due to an asymmetric generation in **k**-space, and under open circuit conditions the open circuit voltage (V_{oc}) is given by:

$$V_{oc} = J_{ph}\rho L \quad (1)$$

where ρ is the resistivity and L is the distance between the electrodes. Moreover, according to Fridkin (Ref. 13) V_{oc} scales inverse proportionally with both dark conductivity and photoconductivity, so that Eq. (1) becomes:

$$V_{oc} = J_{PH}\left(\frac{1}{\sigma_d+\sigma_{ph}}\right)L \quad (2)$$

where σ_d and σ_{ph} are dark conductivity and photoconductivity, respectively.

The exponential-like increase of V_{oc} with decreasing temperature is corroborated by the temperature variation of both dark conductivity and photoconductivity shown in Fig. 5 which represents a direct proof of (1) and (2) for the case of BFO thin films.

As it can be easily seen, both dark and photoconductivity are higher in the case of 109° domains when compared with 71° domains. Also both dark and photoconductivity are higher in the perpendicular than in the parallel geometry. These observations imply firstly that the domain walls have an enhanced conductivity and are largely governing both the dark and photoconductivity of the BFO films. This is not surprising since the dc dark conductivity of 109° DW has been already estimated to be at least four orders of magnitude higher than the bulk of BFO.[20] In the same time the conductivity of 71° DW is lower compared to the 109° DW, which is also in agreement to previous results.[21]

In order to explain the existence and/or absence of the abnormal photovoltaic effect and respectively a value of the open circuit voltage V_{oc} larger than the band gap, we can assume that a photocurrent is rather uniformly generated in the entire film by the photogalvanic effect or, as recently shown using *ab-initio* calculation, by so called "shift currents".[16] In the same time the open circuit voltage is established according to (2) by the actual conductivity of the BFO film considering both the bulk and the domain wall

conductivity. The effective sample conductivity is given by a simple equivalent circuit which is either parallel or serial, depending on the geometrical arrangement of the collecting electrodes relative to the domain walls.

As schematically shown in Fig. 6, in the perpendicular geometry (PPDW) the equivalent circuit is a parallel circuit and the effective conductivity is given by the sum of both bulk and domain wall conductivities $\sigma_{total} = (\sigma_{bulk} + \sigma_{DW})$, whereas in the parallel geometry (PLDW) the appropriate equivalent circuit is the series circuit and in this case the inverse of the effective conductivity is the sum of the inverse conductivities $(\sigma_{total})^{-1} = (\sigma_{bulk})^{-1} + (\sigma_{DW})^{-1}$.

According to this simple model, the effective resistance is lower when the domain walls are running perpendicular to the electrodes and thus the open circuit voltage should be lower in the PPDW geometry. This is valid for all cases (see fig. 5). For 109° domains in which the DW are much more conductive than in 71° domains, the V_{oc} for all the cases was lower than what was measured in cases with 71° domains.

Bulk photovoltaic effect in $BiFeO_3$ films

In order to prove the existence of the bulk PV effect (BPV) in our films we measured the PV current for all the systems by changing the angle between the plane of the linearly polarized light and the direction of current flow. The BPV effect has been studied extensively in non-centrosymmetric materials like $KNbO_3$, $BaTiO_3$, reduced $LiTaO_3$ etc. The BPV effect in ferroelectrics can be expressed in the form of an equation given by [14]

$$\mathbf{J_i} = I\boldsymbol{\beta}_{ijk}\mathbf{e_j}\mathbf{e_k} \quad (3)$$

where $\boldsymbol{\beta}_{ijk}$ is a third rank bulk photovoltaic tensor and I is the intensity of light. According to equation 3, when a homogenous ferroelectric crystal is illuminated uniformly by a linearly polarized light it leads to the generation of a photovoltaic current $\mathbf{J_i}$. The behavior of this photovoltaic current in terms of its sign and magnitude depends on the orientation of the

crystal with respect to the projections of the electric field of the linearly polarized light onto the plane of the sample along X and Y directions, namely $\mathbf{e}_j$ and $\mathbf{e}_k$. Based on equation 3, and as detailed in the Methods, the current generated along the two orthogonal directions X and Y with the light propagating along the Z-direction is given by[14,22,23,24]

$$J_x = -I\beta_{22}\sin 2\theta \text{ and } J_y = I\beta_{22}\cos 2\theta \quad (4)$$

Figure 7a depicts the arrangement of the setup in which the coordinate system shown follows the pseudo cubic notation of the BFO film so that the direction X is given by [001], Y is given by [010] and Z is given by [001]. The light illumination is along the Z [001] direction. For these measurements, the angle 0° means that the **E** vector of the linearly polarized light is parallel to the direction of the current flow, whereas an angle of 90° means that **E** is perpendicular to the current flow direction. The normalized values for the measured photovoltaic current by varying the angle between the current direction and the polarization axis of the light are presented in Figure 7b.

It is rather evident from the plot shown in Figure 7(b) that in either of the systems there is a definitive angular dependency exhibited by the PV current. For both systems studied, the normalized PV current fits the cosine function in (4) proving in this way that the origin of the PV current is the photogalvanic effect. However we must take into consideration that equation 4 is calculated for rhombohedral symmetry. Therefore in order to predict the exact response which we obtain in lab coordinates, the bulk photovoltaic tensor must be transformed from rhombohedral to lab coordinates. We have performed this transformation for 71° domains. The details of this transformation are discussed in the Methods section. The net response obtained in the PLDW geometry can be expressed as

$$J_{\mathrm{PLDW}} = I\left[\frac{\beta_{33}}{3\sqrt{3}} + \frac{2\beta_{31}}{3\sqrt{3}} - \frac{\beta_{22}}{3\sqrt{6}} + \frac{\beta_{15}}{3\sqrt{3}}\right] + I\left[\frac{\beta_{22}}{\sqrt{6}} - \frac{\beta_{15}}{\sqrt{3}}\right]\cos 2\theta \quad (5)$$

flowing in the direction of both ferroelastic distortion and polarization, which is consistent with the theoretical results [16].

Similarly the response in PPDW geometry can be expressed according to the equation

$$J_{\mathrm{PPDW}} = I\left[\frac{\beta_{33}}{3\sqrt{3}} - \frac{\beta_{31}}{3\sqrt{3}} + \frac{2\beta_{22}}{3\sqrt{6}} + \frac{\beta_{15}}{3\sqrt{3}}\right]\sin 2\theta \qquad (6)$$

From equation 5 we can observe that the current collected in PLDW geometry is composed of two components. The second term due to the BPV effect has a cosine dependency and will oscillate depending on angle θ. The first term is also due to the BPV effect but is independent of angle θ. This is also evident when we fit equation 5 to the data we measured in the PLDW geometry as shown in Figure 7c. The θ-dependent behavior of the bulk photovoltaic current is shifted by the non-oscillating 1st term of equation 5. The current in PPDW geometry has a sine dependency on angle θ. However in order to compensate for the combined effects of factors such as misalignments between the electrodes and domains and a misalignment between the light beam direction and the normal to the sample surface we have introduced a phase shift θ_0 and a constant current J_0 to equation 6, which now can be expressed as:

$$J_{\mathrm{PPDW}} = I\left[\frac{\beta_{33}}{3\sqrt{3}} - \frac{\beta_{31}}{3\sqrt{3}} + \frac{2\beta_{22}}{3\sqrt{6}} + \frac{\beta_{15}}{3\sqrt{3}}\right]\sin\left(2\theta + \theta_0\right) + J_0 \qquad (7)$$

From Figure 7d, the agreement between the measured and predicted values from equation 7 is obvious. Based on equation 5-7 and the reported value of β_{22}, we calculated the values of all the bulk photovoltaic coefficients which are as follows β_{15} = -7.1045 x 10^{-5} V^{-1}, β_{31} = -1.17 x 10^{-4} V^{-1} and β_{33} = 9.74 x 10^{-5} V^{-1}. Corresponding values of the glass coefficients are G_{15}=-3.946 x 10^{-10} cm V^{-1}, G_{31}=-6.5 x 10^{-10} cm V^{-1} and G_{33}=5.41 x 10^{-10} cm V^{-1}.

Discussions

We can now explain the scattered behavior in the literature. The most important parameter seems to be the intrinsic conductivity. Samples in any form with high intrinsic conductivity should not show a large V_{oc}. The high conductivity in BFO is a well know problem which might be the result of either unintentional doping of the raw material, or high oxygen vacancy density or any other fabrication parameter. Therefore, only the simple photovoltaic measurement at RT is not sufficient to conclude if a certain material exhibits the anomalous PV effect or not. A detailed complementary analysis of both dark conductivity and photoconductivity, including the temperature analysis and the spectral distribution of the latter (see Figs. S6 and S7), should be performed. In a thin film capacitor (plane-parallel) geometry the film thickness is the most important parameter, as the open circuit voltage scales, according to eq. (1), linearly with it. We would expect to obtain an open circuit voltage of about 0.6 $V\mu m^{-1}$ for the very favorable case shown in Fig. 2(a). Thus to obtain a V_{oc} larger than 3 V the film thickness should be in the range of 5 µm. A large V_{oc} in this geometry is not to be expected for usual sub-micron thicknesses. For a ceramic system, as the conductivity is extrinsic and usually through a grain boundary conduction mechanism, the value of V_{oc} might depend tremendously on the effective fabrication process.

Coming back to the role of the domain walls in the PV in BFO we can state that the domain walls, due to their intrinsically higher conductivity, are rather detrimental for the abnormal PV effect. In normal cases and at room temperature the only geometry which allows high V_{oc} values is that with the domain walls running parallel to the collecting electrodes. If the domain walls are contacting the two collecting electrodes, as in the perpendicular geometry, the expected V_{oc} values are low since the domain walls are acting rather as shunts. Nevertheless, the domain walls proved to show a markedly higher

photoconductivity than the domain bulk. This means that the density of the non-equilibrium carriers generated at the domain walls is much higher than in the bulk, and this might be more significant for photoelectric devices based on BFO than the value of the open circuit voltage.

In summary, by investigating the photovoltaic properties of $BiFeO_3$ thin films in the low temperature range it was observed that above-band-gap open circuit voltages (as large as 50 V) can be obtained irrespective of the domain wall geometry and the type of the domain wall. The open circuit voltages in all the samples and measurement geometries scaled up roughly exponentially with a decrease of temperature. The photogalvanic effect or the shift currents are at the origin of the abnormal photovoltaic effect in BFO. The high dark and photo conductivities of the domain walls are preventing a large open circuit voltage when these are connecting the collecting electrodes.

Acknowledgements

The work was partly funded by DFG *via* SFB 762. A.B. is thankful to IMPRS (International Max Planck Research School, Halle, Germany) for the funding and support. A.R.C. acknowledges the funding from Alexander von Humboldt foundation.

Author contributions

M.A. and A.B. designed and conceived the experiments. A.B. was responsible for thin film growth, PFM analysis and photoelectric measurements. A.R.C. participated in thin film growth. Y.H.K. carried out TEM investigations. M.A., A.B. and D.H. co-wrote the paper.

Competing financial interests

The authors declare no competing financial interests.

Methods

Film Growth

Epitaxial $BiFeO_3$ films of approximately 100 nm thickness were fabricated by pulsed laser deposition technique (PLD). The films were deposited on orthorhombic $TbScO_3$ (110) oriented substrates at 650°C with oxygen pressure of 0.145 mbar. The laser energy was 0.35 Jcm^{-2} and the laser repetition rate was kept at 5 Hz. In order to fabricate films with 109° domains, the deposition was performed on bare $TbScO_3$ substrates. For obtaining 71° domains, the substrates were annealed in a tube furnace at 950°C for 2 hours along with an oxygen flow of approximately 200 sccm[1,25].

Piezoforce microscopy (PFM)

PFM was performed using a.c. excitation signal of 4 V amplitude and 33 kHz frequency applied on the AFM tip. AFM tips with Pt/Ti conductive coating and elastic constants of about 2 Nm^{-1} (NSC14, µMasch) were used.

Photoelectric measurements

The photoelectric effect was measured by illuminating the gap between the electrodes with a 405 nm ($h\upsilon$= 3.06 eV) laser (Newport LQA405-85E) with a maximum power of 80mW and simultaneously measuring the photocurrent using a high-input impedance electrometer (Keithley 6517). Variable temperature measurements were performed using an optical cryostat (Janis VPF-700). Open circuit voltage was extracted from the current-voltage characteristics.

Bulk photovoltaic effect in ferroelectric materials:

BFO belongs to the space group R3c and many of the 27 elements of the third rank tensor will be reduced to zero owing to symmetry operations[26,27,28,29]. The tensor thereafter can be contracted into a 3 by 6 matrix of the form

$$\boldsymbol{\beta}_{ijk} = \begin{bmatrix} 0 & 0 & 0 & 0 & \beta_{15} & -\beta_{22} \\ -\beta_{22} & \beta_{22} & 0 & \beta_{15} & 0 & 0 \\ \beta_{31} & \beta_{31} & \beta_{33} & 0 & 0 & 0 \end{bmatrix} \quad (8)$$

The incident light propagating along the Z-axis can be expressed as [28,29]

$$\mathbf{E} = E_o \exp[i(kz - \omega t)] \quad (9)$$

The electric field vector **E** of the light can be resolved into two components along X and Y axes having *cos* θ and *sin* θ dependencies, respectively.

Hence,

$$\mathbf{E} = E_o\{e_x \cos\theta exp[i(kz - \omega t)] + e_y \sin\theta exp[i(kz - \omega t)]\} \quad (10)$$

$$\mathbf{E} = E_o\{E_1 e_x + E_2 e_y\}$$

where θ is the angle which the polarization axis makes with the direction of current flow. Since **E** is a second rank tensor, it can be expressed in the form of a 6 by 1 matrix and equation (3) takes the form [26, 28]:

$$\mathbf{J_i} = I^* \begin{bmatrix} 0 & 0 & 0 & 0 & \beta_{15} & -\beta_{22} \\ -\beta_{22} & \beta_{22} & 0 & \beta_{15} & 0 & 0 \\ \beta_{31} & \beta_{31} & \beta_{33} & 0 & 0 & 0 \end{bmatrix} * \begin{bmatrix} E_1^2 \\ E_2^2 \\ 0 \\ 0 \\ 0 \\ 2E_1E_2 \end{bmatrix} \quad (11)$$

From (11) we can approximate

$J_x = -I\beta_{22} \sin 2\theta$ and $J_y = I\beta_{22} \cos 2\theta$

Calculation of photovoltaic response:

The bulk photovoltaic tensor $\boldsymbol{\beta_{ijk}}$ is a tensor of third rank. This means it has 3^3 elements. These elements can be expressed as:

$$\boldsymbol{\beta_{ijk}} = \left(\begin{array}{ccc|ccc|ccc} \beta_{111} & \beta_{112} & \beta_{113} & \beta_{211} & \beta_{212} & \beta_{213} & \beta_{311} & \beta_{312} & \beta_{313} \\ \beta_{121} & \beta_{122} & \beta_{123} & \beta_{221} & \beta_{222} & \beta_{223} & \beta_{321} & \beta_{322} & \beta_{323} \\ \beta_{131} & \beta_{132} & \beta_{133} & \beta_{231} & \beta_{232} & \beta_{233} & \beta_{331} & \beta_{323} & \beta_{333} \end{array}\right) \quad (12)$$

Since the projections of the electric field vector of the light ($\mathbf{e_j}\,\mathbf{e_k}$) are symmetric with respect to each other, it means that the BPV tensor can be assumed to be symmetrical in j and k [27, 29]. Due to this symmetry aspect, there remain only 18 independent $\boldsymbol{\beta_{ijk}}$ coefficients which can be conveniently represented in a matrix notation of the form:

$$\boldsymbol{\beta_{ijk}} = \begin{bmatrix} \beta_{11} & \beta_{12} & \beta_{13} & \beta_{14} & \beta_{15} & \beta_{16} \\ \beta_{21} & \beta_{22} & \beta_{23} & \beta_{24} & \beta_{25} & \beta_{26} \\ \beta_{31} & \beta_{32} & \beta_{33} & \beta_{34} & \beta_{35} & \beta_{36} \end{bmatrix} \quad (13)$$

The coefficients in equation (12) are related to the coefficients in equation (13) in such an arrangement that the first suffix remains the same in both the notations, whereas the last two notations are related according to the following relations [27]:

Tensor notation :	11	22	33	23, 32	31,13	12, 21
Matrix notation:	1	2	3	4	5	6

However, there is a further reduction in the number of independent tensor coefficients due to the R3c symmetry of $BiFeO_3$ (BFO). Henceforth, the matrix in equation (7) is reduced to [27, 28]:

$$\boldsymbol{\beta_{ijk}} = \begin{bmatrix} 0 & 0 & 0 & 0 & \beta_{15} & -\beta_{22} \\ -\beta_{22} & \beta_{22} & 0 & \beta_{15} & 0 & 0 \\ \beta_{31} & \beta_{31} & \beta_{33} & 0 & 0 & 0 \end{bmatrix} \quad (14)$$

It can be observed by comparing equation (13) and (14) that, $\beta_{22} = -\beta_{21} = -\beta_{16}$, $\beta_{15} = \beta_{24}$ and $\beta_{31} = \beta_{32}$ [27]. Therefore the bulk photovoltaic effect in BFO can be completely described by the

help of four independent coefficients which are $\beta_{15,}\beta_{22,}\beta_{31}$ and β_{33}. By using equation (14) and the matrix notations, we know that

$$\begin{aligned}
&\beta_{15} = \beta_{24} = \beta_{113} = \beta_{131} = \beta_{223} = \beta_{232} \\
&\beta_{22} = -\beta_{21} = -\beta_{16} = \beta_{222} = -\beta_{211} = -\beta_{112} = -\beta_{121} \\
&\beta_{31} = \beta_{32} = \beta_{311} = \beta_{322} \\
&\beta_{33} = \beta_{333}
\end{aligned} \tag{15}$$

Based on the relations given in (15), we can rewrite equation (12) to obtain a third rank tensor which would be valid for BFO:

$$\boldsymbol{\beta}_{\mathbf{ijk}} = \left(\begin{array}{ccc|ccc|ccc}
0 & -\beta_{112} & \beta_{113} & -\beta_{211} & 0 & 0 & \beta_{311} & 0 & 0 \\
-\beta_{121} & 0 & 0 & 0 & \beta_{222} & \beta_{223} & 0 & \beta_{322} & 0 \\
\beta_{131} & 0 & 0 & 0 & \beta_{232} & 0 & 0 & 0 & \beta_{333}
\end{array}\right) \tag{16}$$

In order to predict the PV current which we measure in lab coordinates we must convert the BPV tensor from rhombohedral to lab coordinates. Additionally, a film comprising of 71° domains, as shown in Supplementary Figure S5, consists of two kinds of rhombohedral unit cells which results in two different domains. These have been shown as R-type and L-type in Supplementary Figure S5.

Therefore such a conversion must be performed for both the cells and domains. The matrices which are required to transform the rhombohedral coordinate system of the R-and L-type domains to lab coordinates are given by [16]:

$$\mathbf{R} = \begin{bmatrix}
-\frac{1}{\sqrt{2}} & \frac{1}{\sqrt{6}} & \frac{1}{\sqrt{3}} \\
\frac{1}{\sqrt{2}} & \frac{1}{\sqrt{6}} & \frac{1}{\sqrt{3}} \\
0 & \frac{2}{\sqrt{6}} & -\frac{1}{\sqrt{3}}
\end{bmatrix} \tag{17}$$

$$\mathbf{L}=\begin{bmatrix} -\frac{1}{\sqrt{2}} & -\frac{1}{\sqrt{6}} & -\frac{1}{\sqrt{3}} \\ -\frac{1}{\sqrt{2}} & \frac{1}{\sqrt{6}} & \frac{1}{\sqrt{3}} \\ 0 & \frac{2}{\sqrt{6}} & -\frac{1}{\sqrt{3}} \end{bmatrix} \tag{18}$$

The BPV tensor in the lab coordinates can then be expressed as a resultant of both the conversions:

$$\mathbf{B_{qrs}}=\left(\mathbf{R_{qi}R_{rj}R_{sk}\beta_{ijk}}+\mathbf{L_{qi}L_{rj}L_{sk}\beta_{ijk}}\right)/2 \tag{19}$$

Based on the non-zero terms in equation (16), we can elaborate equation (19) as:

$$\mathbf{B_{qrs}}=\begin{pmatrix} -\mathbf{R_{q1}R_{r1}R_{s2}}\beta_{112}-\mathbf{R_{q1}R_{r2}R_{s1}}\beta_{121}+\mathbf{R_{q1}R_{r1}R_{s3}}\beta_{113}+\mathbf{R_{q1}R_{r3}R_{s1}}\beta_{131} \\ -\mathbf{R_{q2}R_{r1}R_{s1}}\beta_{211}+\mathbf{R_{q2}R_{r2}R_{s2}}\beta_{222}+\mathbf{R_{q2}R_{r2}R_{s3}}\beta_{223}+\mathbf{R_{q2}R_{r3}R_{s2}}\beta_{232} \\ +\mathbf{R_{q3}R_{r1}R_{s1}}\beta_{311}+\mathbf{R_{q3}R_{r2}R_{s2}}\beta_{322}+\mathbf{R_{q3}R_{r3}R_{s3}}\beta_{333}-\mathbf{L_{q1}L_{r1}L_{s2}}\beta_{112} \\ -\mathbf{L_{q1}L_{r2}L_{s1}}\beta_{121}+\mathbf{L_{q1}L_{r1}L_{s3}}\beta_{113}+\mathbf{L_{q1}L_{r3}L_{s1}}\beta_{131}-\mathbf{L_{q2}L_{r1}L_{s1}}\beta_{211}+ \\ \mathbf{L_{q2}L_{r2}L_{s2}}\beta_{222}+\mathbf{L_{q2}L_{r2}L_{s3}}\beta_{223}+\mathbf{L_{q2}L_{r3}L_{s2}}\beta_{232}+\mathbf{L_{q3}L_{r1}L_{s1}}\beta_{311} \\ +\mathbf{L_{q3}L_{r2}L_{s2}}\beta_{322}+\mathbf{L_{q3}L_{r3}L_{s3}}\beta_{333} \end{pmatrix}/2 \tag{20}$$

From the relations given in (15) we can rearrange equation (20) to

$$\begin{aligned} \mathbf{B_{qrs}}=&\frac{1}{2}\beta_{15}\begin{pmatrix}\mathbf{R_{q1}R_{r1}R_{s3}}+\mathbf{R_{q1}R_{r3}R_{s1}}+\mathbf{R_{q2}R_{r2}R_{s3}}+\mathbf{R_{q2}R_{r3}R_{s2}} \\ +\mathbf{L_{q1}L_{r1}L_{s3}}+\mathbf{L_{q1}L_{r3}L_{s1}}+\mathbf{L_{q2}L_{r2}L_{s3}}+\mathbf{L_{q2}L_{r3}L_{s2}}\end{pmatrix} \\ &+\frac{1}{2}\beta_{22}\begin{pmatrix}-\mathbf{R_{q1}R_{r1}R_{s2}}-\mathbf{R_{q1}R_{r2}R_{s1}}-\mathbf{R_{q2}R_{r1}R_{s1}}+\mathbf{R_{q2}R_{r2}R_{s2}} \\ -\mathbf{L_{q1}L_{r1}L_{s2}}-\mathbf{L_{q1}L_{r2}R_{s1}}-\mathbf{L_{q2}L_{r1}L_{s1}}+\mathbf{L_{q2}L_{r2}L_{s2}}\end{pmatrix} \\ &+\frac{1}{2}\beta_{31}\left(\mathbf{R_{q3}R_{r1}R_{s1}}+\mathbf{R_{q3}R_{r2}R_{s2}}+\mathbf{L_{q3}L_{r1}L_{s1}}+\mathbf{L_{q3}L_{r2}L_{s2}}\right) \\ &+\frac{1}{2}\beta_{33}\left(\mathbf{R_{q3}R_{r3}R_{s3}}+\mathbf{L_{q3}L_{r3}L_{s3}}\right) \end{aligned} \tag{21}$$

Having calculated the BPV tensor in lab coordinates we can now predict the PV current in lab coordinates by

$$\mathbf{J_q}=I\mathbf{B_{qrs}E_rE_s} \tag{22}$$

The projections of the electric field of a linearly polarized light can be resolved into a second rank tensor via Jones matrix notation. This matrix can then be written in a (6x1) form of the

type $\left[\cos^2\theta, \sin^2\theta, 0, 0, 0, 2\sin\theta\cos\theta\right]$. Also, as explained previously, we can reduce the lab BPV tensor ($\mathbf{B_{qrs}}$) to a matrix notation of (3x6) type. Therefore we can solve equation (22) by simple matrix multiplication with the result being of the type:

$$\begin{bmatrix} J_{\mathrm{PPDW}} \\ J_{\mathrm{PLDW}} \\ J_{\mathrm{Z}} \end{bmatrix} = I \begin{bmatrix} B_{12}\sin^2\theta + 2B_{16}\sin\theta\cos\theta + B_{11}\cos^2\theta \\ B_{22}\sin^2\theta + 2B_{26}\cos\theta\sin\theta + B_{21}\cos^2\theta \\ B_{32}\sin^2\theta + 2B_{36}\cos\theta\sin\theta + B_{31}\cos^2\theta \end{bmatrix} \tag{23}$$

As can be observed from equation (23), the main coefficients required to predict the PV current in PPDW and PLDW geometries are B_{12}, B_{16}, B_{11}, B_{22}, B_{26}, B_{21}. By substituting the values from equation (17) and (18) (using relation given in 15) into equation (21) we can calculate these terms to be:

$$B_{12} = 0 \tag{24}$$

$$B_{16} = \frac{\beta_{33}}{3\sqrt{3}} - \frac{\beta_{31}}{3\sqrt{3}} + \frac{2\beta_{22}}{3\sqrt{6}} + \frac{\beta_{15}}{3\sqrt{3}} \tag{25}$$

$$B_{11} = 0 \tag{26}$$

$$B_{22} = \frac{\beta_{33}}{3\sqrt{3}} + \frac{2\beta_{31}}{3\sqrt{3}} - \frac{4\beta_{22}}{3\sqrt{6}} + \frac{4\beta_{15}}{3\sqrt{3}} \tag{27}$$

$$B_{26} = 0 \tag{28}$$

$$B_{21} = \frac{\beta_{33}}{3\sqrt{3}} + \frac{2\beta_{31}}{3\sqrt{3}} + \frac{2\beta_{22}}{3\sqrt{6}} - \frac{2\beta_{15}}{3\sqrt{3}} \tag{29}$$

By substituting the values of the coefficients from equations (24)-(29) in equation (23), the calculated PV current in the direction which is parallel to the domains is:

$$J_{\mathrm{PLDW}} = I\left[\frac{\beta_{33}}{3\sqrt{3}} + \frac{2\beta_{31}}{3\sqrt{3}} + \frac{2\beta_{15}}{3\sqrt{3}}\left(-\cos 2\theta + \sin^2\theta\right) - \frac{2\beta_{22}}{3\sqrt{6}}\left(-\cos 2\theta + \sin^2\theta\right)\right] \tag{30}$$

Equation (30) can be further simplified by applying trigonometric operations resulting in

$$J_{\mathrm{PLDW}} = I\left[\frac{\beta_{33}}{3\sqrt{3}} + \frac{2\beta_{31}}{3\sqrt{3}} - \frac{\beta_{22}}{3\sqrt{6}} + \frac{\beta_{15}}{3\sqrt{3}}\right] + I\left[\frac{\beta_{22}}{\sqrt{6}} - \frac{\beta_{15}}{\sqrt{3}}\right]\cos 2\theta \tag{31}$$

The calculated PV current in the direction which is perpendicular to the domains is:

$$J_{\mathrm{PPDW}} = I\left[\frac{\beta_{33}}{3\sqrt{3}} - \frac{\beta_{31}}{3\sqrt{3}} + \frac{2\beta_{22}}{3\sqrt{6}} + \frac{\beta_{15}}{3\sqrt{3}}\right]\sin 2\theta \qquad (32)$$

References

[1] Yang, S. Y. *et al.* Above-bandgap voltages from ferroelectric photovoltaic devices. *Nature nanotechnology* **5**, 143–147 (2010).
[2] Guo, R., You, L., Chen, L., Wu, D. & Wang, J. Photovoltaic property of $BiFeO_3$ thin films with 109° domains. *Applied Physics Letters* **99**, 122902 (2011).
[3] Yang, S. Y. *et al.* Photovoltaic effects in $BiFeO_3$. *Applied Physics Letters* **95**, 062909 (2009).
[4] Lee, D. *et al.* Polarity control of carrier injection at ferroelectric/metal interfaces for electrically switchable diode and photovoltaic effects. *Physical Review* B **84**, 125305 (2011).
[5] Alexe, M. & Hesse, D. Tip-enhanced photovoltaic effects in bismuth ferrite. *Nature Communications* **2**, 256 (2011).
[6] Choi, T., Lee, S., Choi, Y. J., Kiryukhin, V. & Cheong, S.-W. Switchable ferroelectric diode and photovoltaic effect in $BiFeO_3$. *Science (New York, N.Y.)* **324**, 63–66 (2009).
[7] Moubah, R. *et al.* Photoelectric Effects in Single Domain $BiFeO_3$ Crystals. *Advanced Functional Materials* **22**, 4814–4818 (2012).
[8] Seidel, J. *et al.* Efficient Photovoltaic Current Generation at Ferroelectric Domain Walls. *Physical Review Letters* **107**, 126805 (2011).
[9] Chynoweth, A.G. Surface space-charge layers in Barium Titanate. Phys. Rev. **102**, 705-714 (1956).
[10] Koch, W.T.H. *et.al.* Bulk photovoltaic effect in $BaTiO_3$, Solid State Comm. **17**, 847-850 (1975).
[11] Koch, W.T.H. *et.al.* Anomalous photo voltage in $BaTiO_3$, Ferroelectrics **13**, 305-307 (1975).
[12] Glass, A. M., Linde, D. von der & Negran, T. J. High-voltage bulk photovoltaic effect and the photorefractive process in LiNbO3. *Applied Physics Letters* **25**, 233 (1974).
[13] Fridkin, V. M. Photoferroelectrics. *Springer-Verlag* Berlin Heidelberg New York, (1979)
[14] Sturman, B. I. & Fridkin, V. M. *The Photovoltaic and Photorefractive Effects in Noncentrosymmetric Materials*. Gordon and Breach Science ,21–37 (1992).
[15] Alexe, M. Local mapping of generation and recombination lifetime in $BiFeO_3$ single crystals by scanning probe photoinduced transient spectroscopy. *Nano letters* **12**, 2193–2198 (2012).
[16] Young, S. M., Zheng, F. & Rappe, A. M. First-Principles Calculation of the Bulk Photovoltaic Effect in Bismuth Ferrite. *Physical Review Letters* **109**, 236601 (2012).
[17] R. von Baltz and W. Kraut. Theory of the bulk photovoltaic effect in pure crystals. *Physical Review* B **23**, 5590 (1981).
[18] Belinicher, V. I. and Sturman, B. I. The photogalvanic effect in media lacking a center of symmetry. *Sov. Phys. Usp.* **23**, 199-223 (1980)
[19] Ruppel, W., Baltz, R. von. and Würfel, P. The origin of the photo-EMF in ferroelectric and non-ferroelectric materials. *Ferroelectrics* **43**, 109-123 (1982).
[20] He, Q. *et al.* Magnetotransport at Domain Walls in $BiFeO_3$. *Physical Review Letters* **108**, 1–5 (2012).
[21] Chiu, Y.-P. *et al.* Atomic-scale evolution of local electronic structure across multiferroic domain walls. *Advanced materials (Deerfield Beach, Fla.)* **23**, 1530–1534 (2011).
[22] Ji, W., Yao, K. & Liang, Y. C. Evidence of bulk photovoltaic effect and large tensor coefficient in ferroelectric $BiFeO_3$thin films. *Physical Review B* **84**, 094115 (2011).
[23] Festl, H. G., Hertel, P., Krätzig, E. & von Baltz, R. Investigations of the Photovoltaic Tensor in Doped $LiNbO_3$. *physica status solidi (b)* **113**, 157–164 (1982).
[24] Avakyan, E.M., Belabaev, K.G., Odulov, S.G. and Oleinik, O.I. Photogalvanic currents in reduced Lithium-Titanate crystals. Izvestiya Akademii Nauk SSSR. Seriya Fizicheskaya **47**, 656-659 (1983).
[25] Johann, F., Morelli, A. & Vrejoiu, I. Stability of 71° stripe domains in epitaxial $BiFeO_3$ films upon repeated electrical switching. *Physica Status Solidi (B)* **249**, 2278–2286 (2012).
[26] Wilson, D. W., Glytsis, E. N., Hartman, N. F. & Gaylord, T. K. Beam diameter threshold for polarization conversion photoinduced by spatially oscillating bulk photovoltaic currents in $LiNbO_3$: Fe. *Journal of the Optical Society of America B* **9**, 1714 (1992).
[27] Nye, J. F. *Physical properties of crystals*. Oxford University Press, (1960).
[28] R.E.Newnham, Properties of materials, Oxford University Press, 2005.

[29] Weis, R. S. & Gaylord, T. K. Lithium Niobate: Summary of Physical Properties and Crystal Structure. *Applied Physics A* **37**, 191–203 (1985).

Figure captions

Figure 1. **Domain configurations.** PFM images (3.5 x 3.5 μm scan) of pristine sample with 71° domains, (a) out of plane phase image (b) in-plane phase image showing stripes which run along $[001]_o$. (c) 2-beam bright-field TEM image of a BFO epitaxial film grown on TSO taken with near **g** = 001_c. The dark and bright contrasts show the domain structure of the BFO thin film. The type of domains was identified as 109° stripe domains with $(100)_c$ vertical domain walls. (d) The high resolution TEM image corresponding to figure 1(c) shows coherency on either side of the vertical domain wall and the two polarization variants.

Figure 2. **Measurement geometries.** Schematic showing the patterned electrodes on top of a film with majority 71° domains (not to scale) and typical measurement geometries in which the electrodes are running: (a) parallel (PLDW) and (b) perpendicular to domain walls (PPDW), respectively. The arrows indicate the direction of polarization in out-of-plane (up-down) and in-plane (left-right) directions.

Figure 3. **Abnormal photovoltaic effect.** I-V characteristics under illumination with monochromatic light ($h\upsilon$=3.05 eV) of BFO thin films comprising (a) 109° and (b) 71° periodic stripe domains.

Figure 4. **Temperature dependent V_{oc}.** Temperature dependence of the open circuit voltage for 109° DW in (a) perpendicular and (c) parallel geometry and for 71° DW in (b) perpendicular and (d) parallel geometry for two gap widths, i.e. 15 μm and 100 μm.

Figure 5. **Conductivity measurement.** Temperature dependence of dark conductivity (a, b) and photoconductivity (c, d) measured with the electrodes running perpendicular (PPDW) and parallel (PLDW) to the domain walls for both 109° and 71° domains.

Figure 6. **Two resistance model.** A schematic showing the periodic arrangement of domains and domain walls in BFO thin films for the (a) parallel (PLDW) and (c) perpendicular (PPDW) geometry with respect to the domain walls. An equivalent circuit considering that the

domain bulk and domain walls have different resistances, R_{bulk} and R_{DW}, is shown for both the geometries in (b) PLDW and (d) PPDW.

Figure 7. **Bulk photovoltaic effect.** (a) Schematic of a sample showing stripes which represent the domain walls either of the 109° or 71° stripe domain system. The coordinate system is given by XYZ. The schematic shows how the vector **E** of the linearly polarized light is aligned with the direction of the current flow *J* for the PLDW case. (b) Normalized photovoltaic current measured at different angles (θ) which the polarization axis of the linearly polarized light makes with the direction of the current flow in the PLDW geometry for samples with 71° (-■-) and 109° (-●-) domains, respectively. The solid line represents the fit with eq. 4. Photovoltaic current measured and predicted by varying the angle θ that the light polarization axis makes with the direction of current flow in c) PLDW geometry and d) PPDW geometry for a film consisting of 71° domains. In all the plots a 5% (rough estimate) error has been incorporated in the PV current measurement to compensate for any misalignment in laser beam spot positioning.

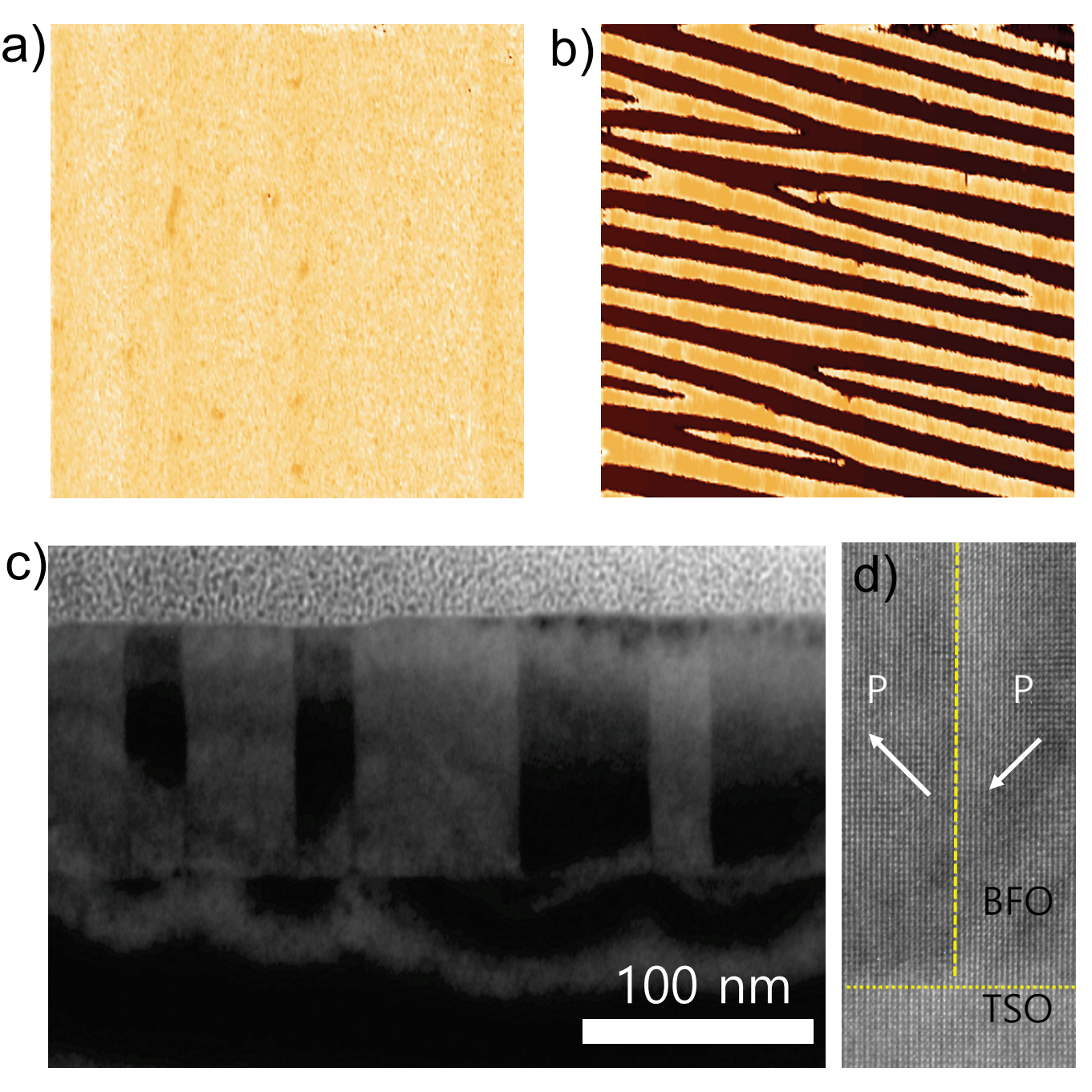
a)
b)
c)
100 nm
d)
P
P
BFO
TSO

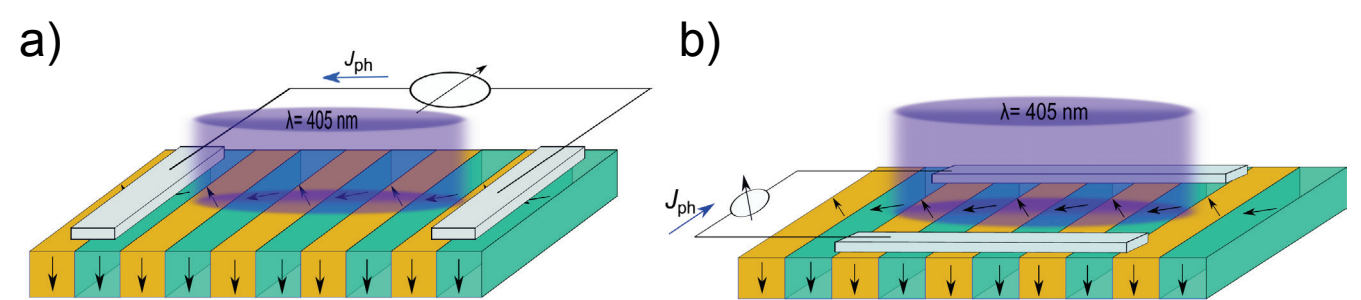
a)
J_{ph}
λ= 405 nm
b)
λ= 405 nm
J_{ph}

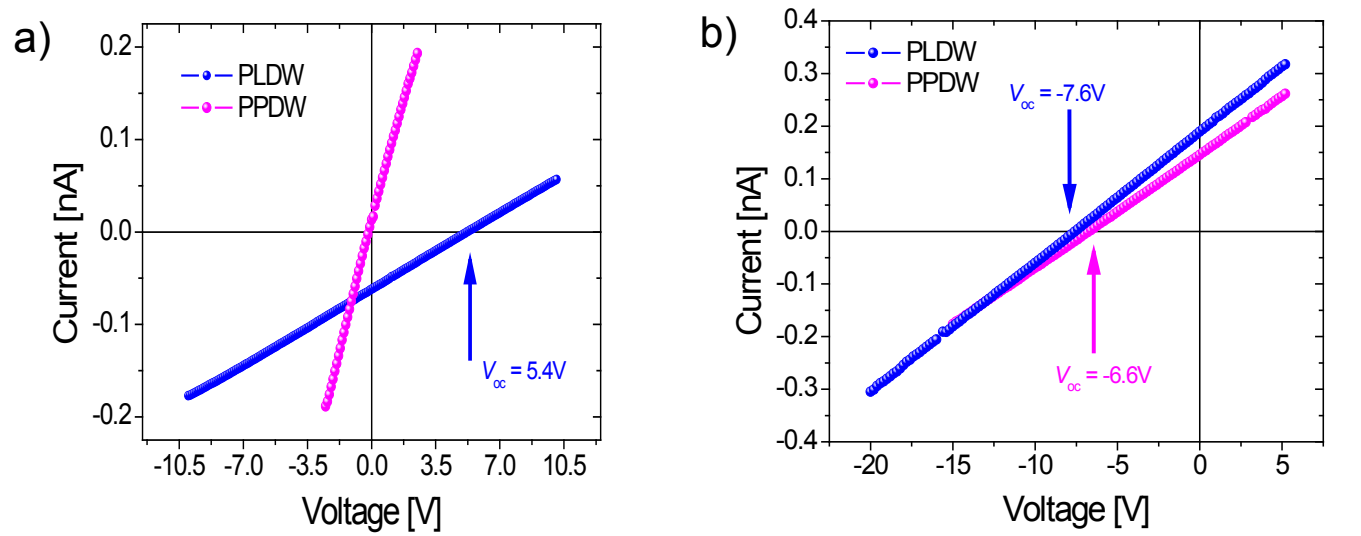
a)
PLDW
PPDW
Current [nA]
Voltage [V]
V_{oc} = 5.4V
b)
PLDW
PPDW
V_{oc} = -7.6V
V_{oc} = -6.6V
Current [nA]
Voltage [V]

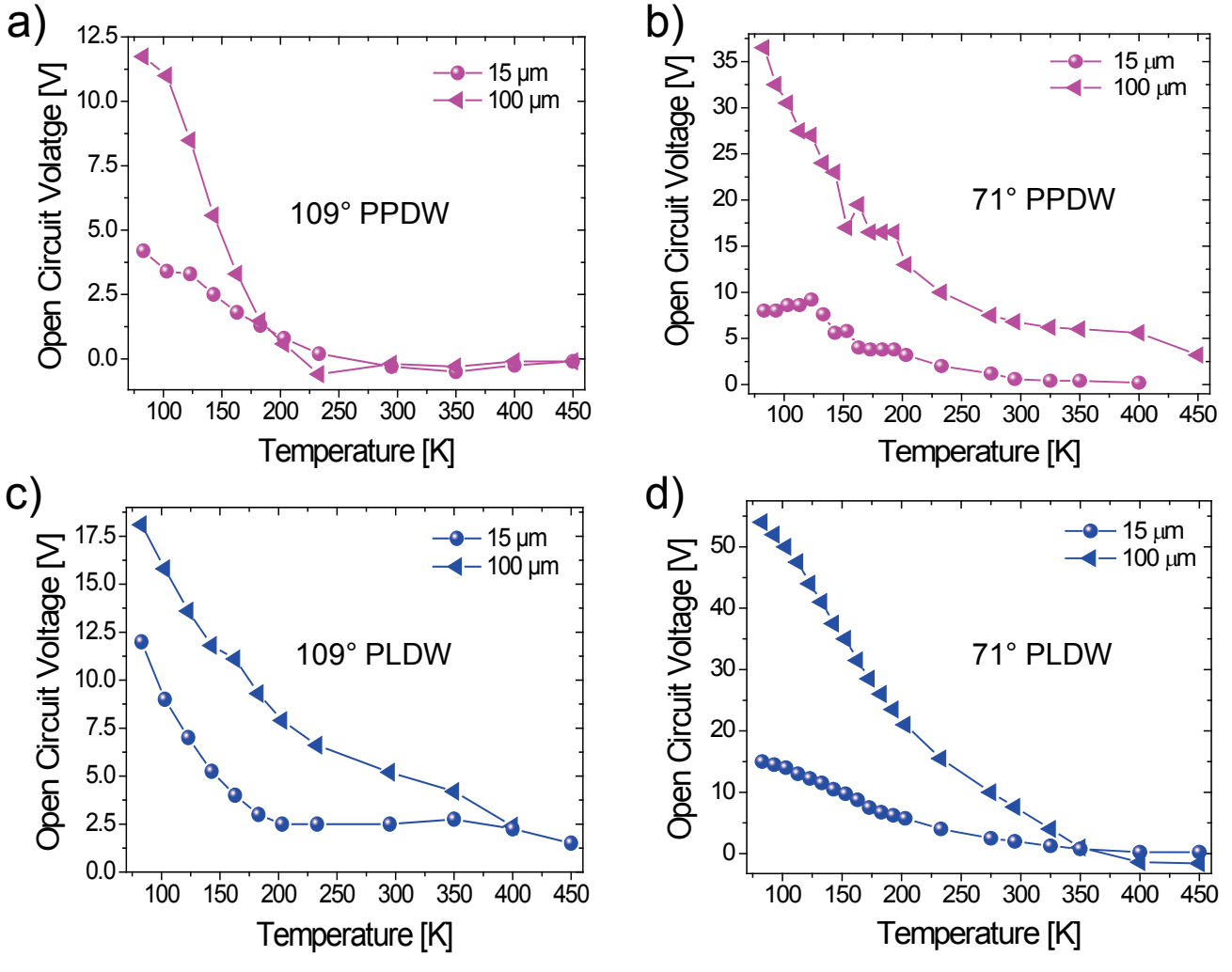
a)
Open Circuit Volatge [V]
Temperature [K]
15 µm
100 µm
109° PPDW
b)
Open Circuit Voltage [V]
Temperature [K]
15 µm
100 µm
71° PPDW
c)
Open Circuit Voltage [V]
Temperature [K]
15 µm
100 µm
109° PLDW
d)
Open Circuit Voltage [V]
Temperature [K]
15 µm
100 µm
71° PLDW

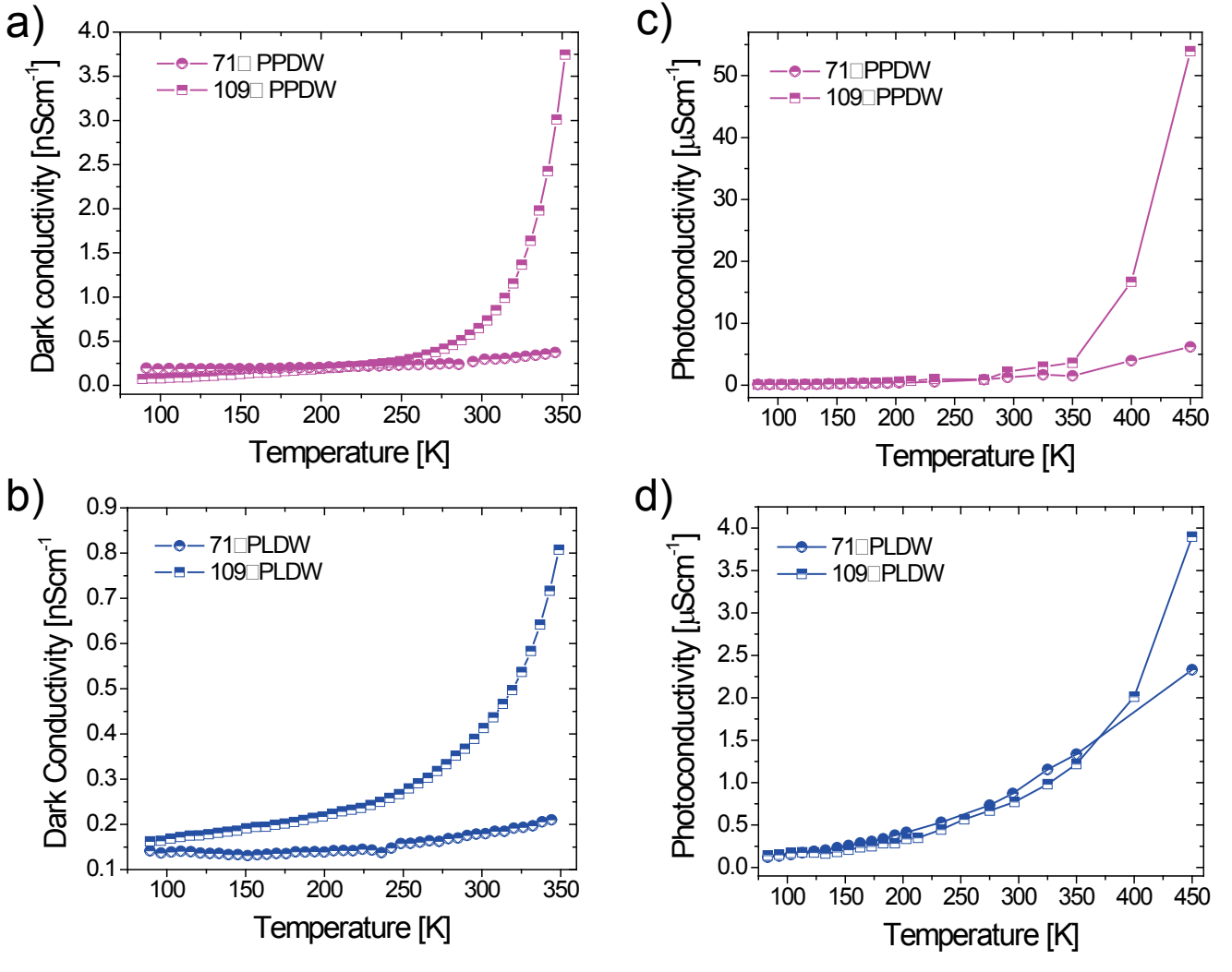
a)
Dark conductivity [nScm^{-1}]
71□ PPDW
109□ PPDW
Temperature [K]
b)
Dark Conductivity [nScm^{-1}]
71□PLDW
109□PLDW
Temperature [K]
c)
Photoconductivity [μScm^{-1}]
71□PPDW
109□PPDW
Temperature [K]
d)
Photoconductivity [μScm^{-1}]
71□PLDW
109□PLDW
Temperature [K]

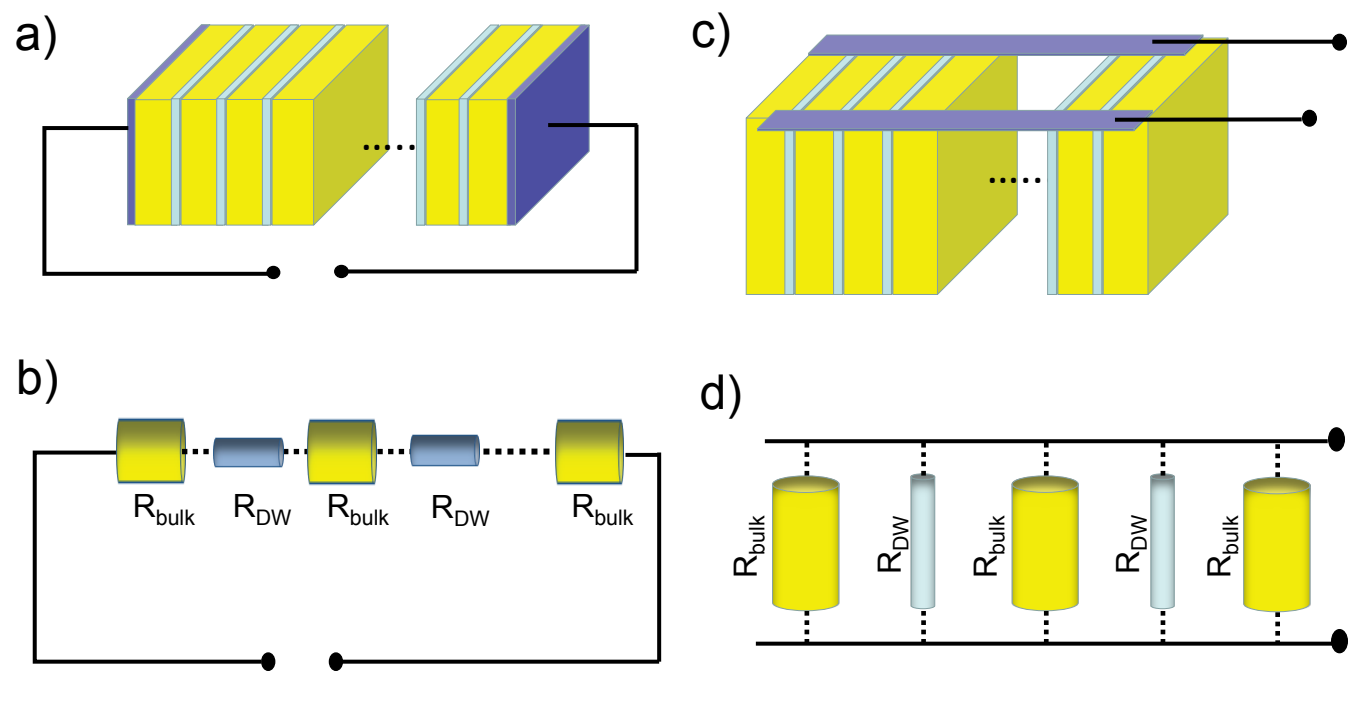
a)
c)
b)
d)
R_{bulk}
R_{DW}
R_{bulk}
R_{DW}
R_{bulk}
R_{bulk}
R_{DW}
R_{bulk}
R_{DW}
R_{bulk}

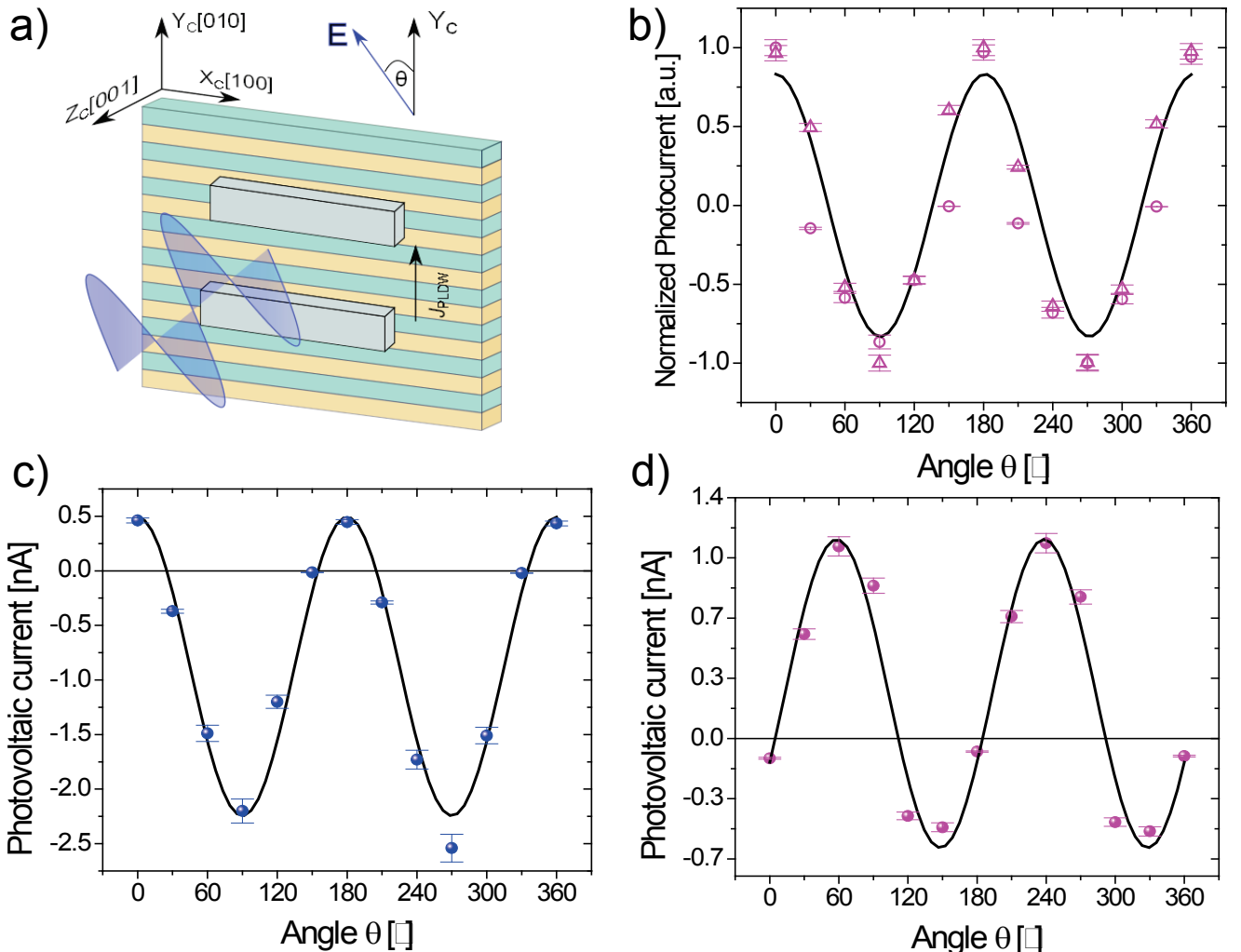
a)
Yc[010]
Xc[100]
Zc[001]
E
Yc
θ
JPLDW
b)
Normalized Photocurrent [a.u.]
1.0
0.5
0.0
-0.5
-1.0
0
60
120
180
240
300
360
Angle θ [°]
c)
Photovoltaic current [nA]
0.5
0.0
-0.5
-1.0
-1.5
-2.0
-2.5
0
60
120
180
240
300
360
Angle θ [°]
d)
Photovoltaic current [nA]
1.4
1.0
0.7
0.3
0.0
-0.3
-0.7
0
60
120
180
240
300
360
Angle θ [°]

Supplementary online material

Role of domain walls in the abnormal photovoltaic effect in $BiFeO_3$

Akash Bhatnagar, Ayan Roy Chaudhuri , Young Heon Kim, Dietrich Hesse, and Marin Alexe

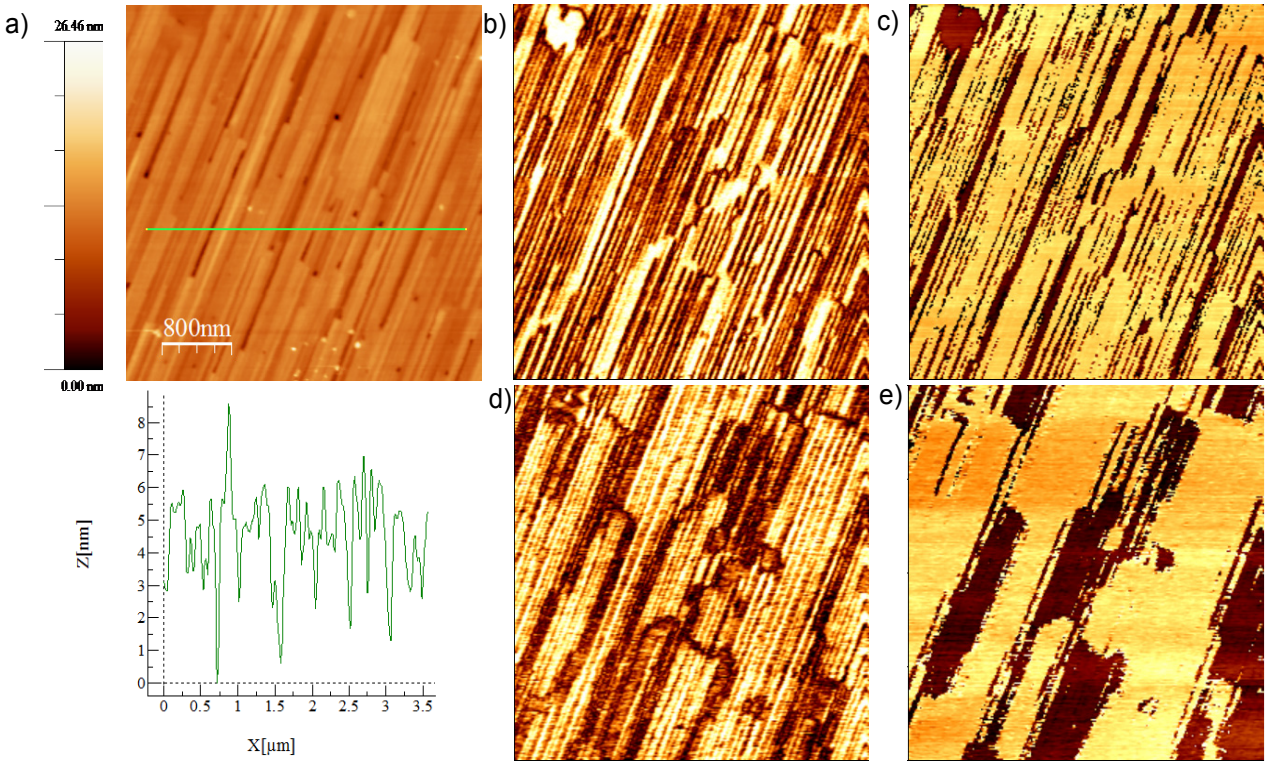

Supplementary Figure S1. AFM and PFM. Atomic and piezo force microscopy (AFM/PFM) images (4 x 4 μm) showing a periodic domain pattern in a sample with 109° domains. a) Topography and line scan profile along X and Y directions. Out-of-plane (OOP) PFM signal: b) amplitude, and c) phase. In-plane (IP) PFM signal: d) amplitude, and e) phase.

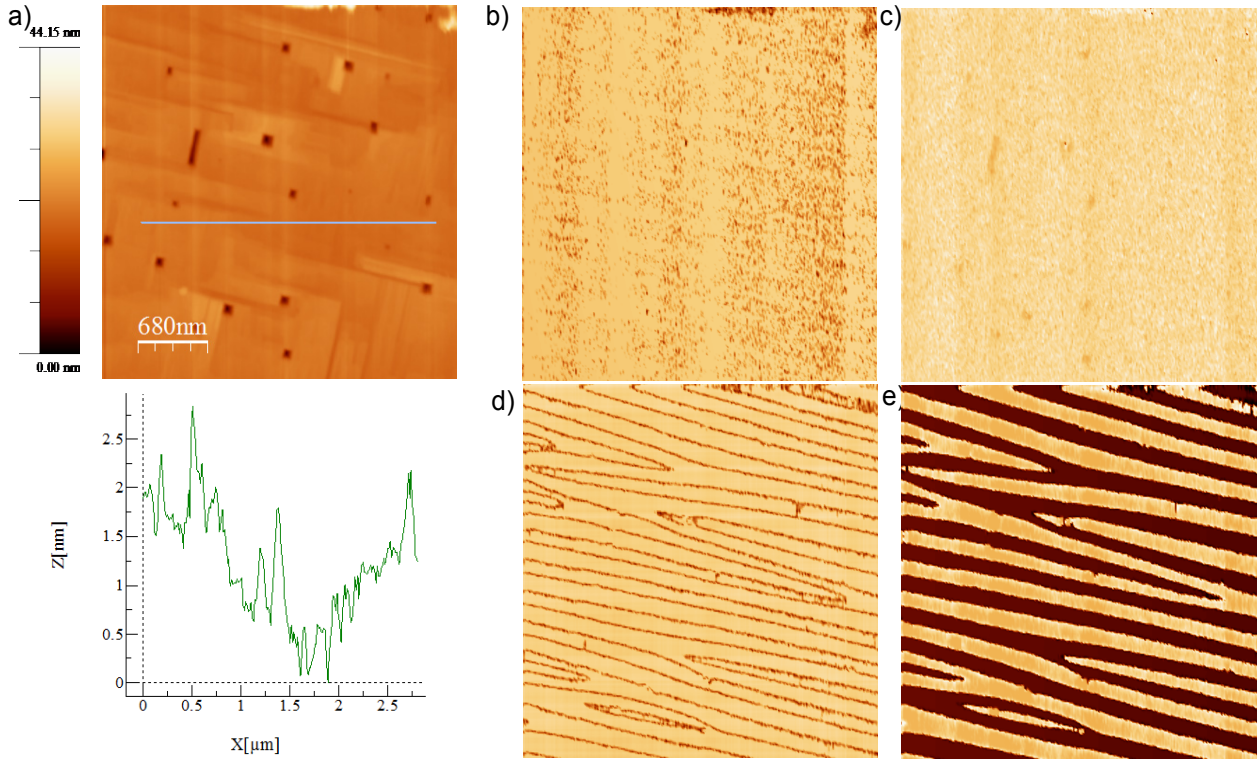

Supplementary Figure S2. AFM and PFM. Atomic and piezo force microscopy (AFM/PFM) images (3.5 x 3.5 µm) showing a periodic domain pattern in a sample with 71° domains. a) Topography and line scan profile along X and Y directions. Out-of-plane (OOP) PFM signal: b) amplitude, and c) phase. In-plane (IP) PFM signal: d) amplitude, and e) phase.

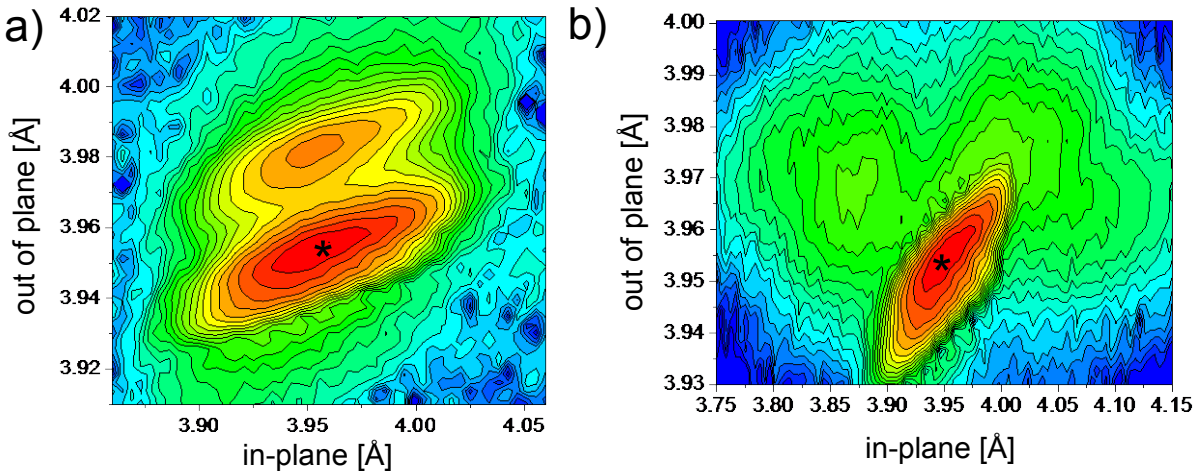

Supplementary Figure S3. Reciprocal space maps. XRD-Reciprocal space maps around the $(103)_{pc}$ peak of $BiFeO_3$ films grown on $TbScO_3$ (110). Films with a thickness of 100 nm and with a) 71° and b) 109° domains were measured. The substrate peaks have been marked with a star.

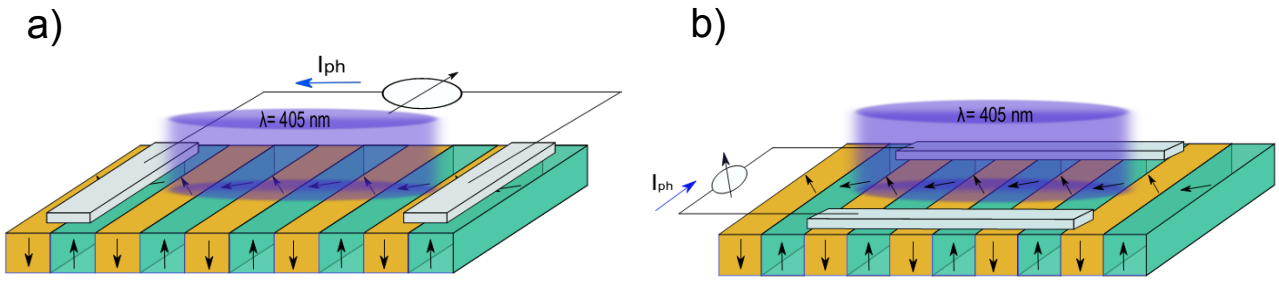

Supplementary Figure S4. Measurement geometries. Schematic showing, on an exaggerated scale, the patterned electrodes on top of a film with majority 109° domains. The arrows indicate the direction of polarization in out of plane (up-down) and in-plane (left-right) directions, *viz.* a) when the electrodes are running parallel to the domain walls (PLDW), and (b) when the electrodes are perpendicular to the domain wall (PPDW).

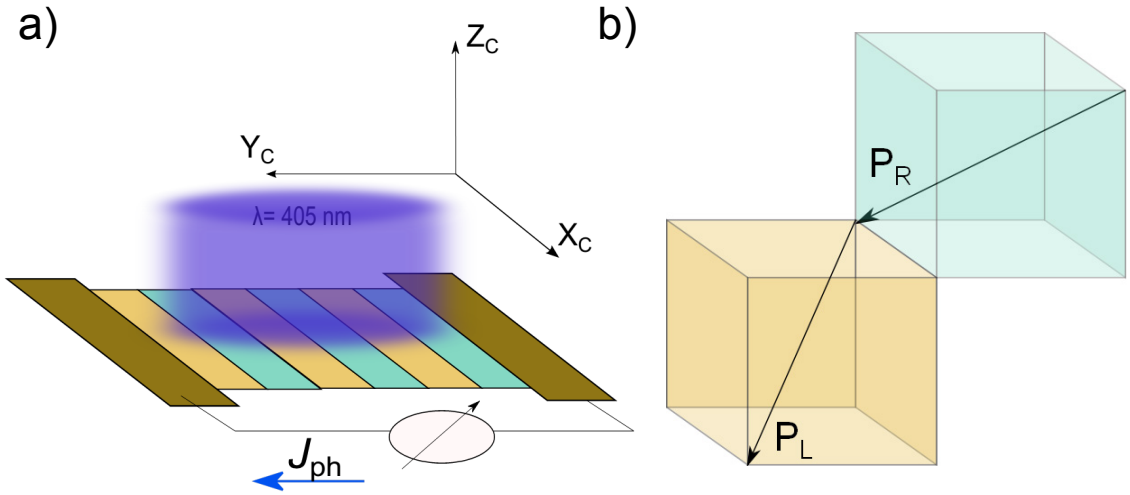

Supplementary Figure S5. Polarization orientation in a 71° domain film. a) Schematic of the measurement geometry for a sample with alternating 71° domains parallel to the electrodes (PLDW) along with the lab coordinate system. b) Pseudo cubic schematic of two kinds of domains in a sample with 71° domains. P_R and P_L show the direction of polarization for the two kinds of domain.

Spectral distribution of the photocurrent

The response we measured per light intensity on our samples is shown in Figure S6. We used a white light source along with a monochromator and measured the photocurrent as a function of different wavelengths. The photoconductive (PC) response we obtained from our samples is largely in agreement with the results obtained from first principle calculations [16]. The peak in the spectral distribution of the PC response is approximately 2.85 eV which is 0.08 eV higher than previously reported values[29]. Interestingly, it can be noted from Figure S6 that there is a significant increase in measured response at an energy approx. 2.4 eV which indicates the presence of shallow trap levels or sub-band levels just below the conduction band [15]. The trap levels in the band gap and the asymmetry of the structure are necessary conditions for the bulk photovoltaic effect, as it has been specifically stated in early theoretical work of Ruppel et al [19].

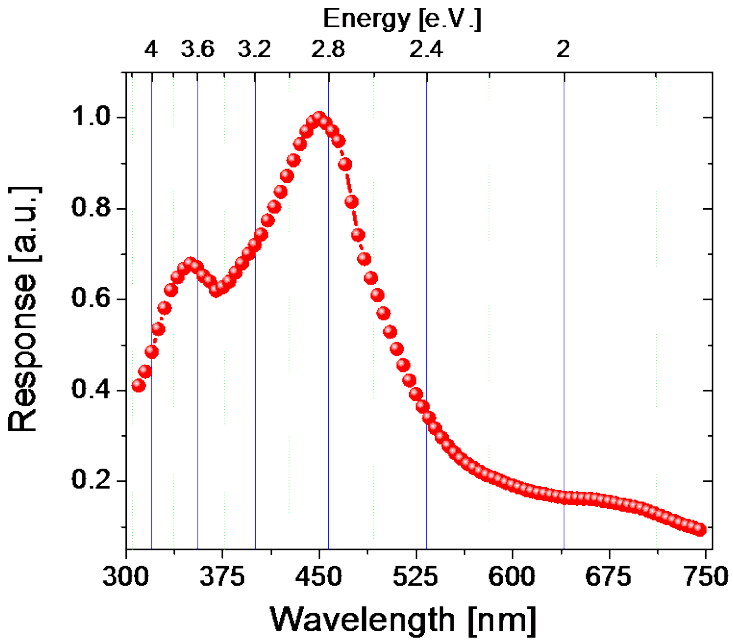

Supplementary Figure S6. Spectral distribution. Normalized spectral distribution of the photocurrent response of a BFO film.

Relationship between conductivity behavior and V_{oc} values:

In order to predict the open circuit voltage (V_{OC}) values we have used the expression

$$V_{OC} = J_{ph}\left(\frac{1}{\sigma_d + \sigma_{ph}}\right)L \qquad (1)$$

From our measurements we found that both dark (σ_d) and photo conductivity (σ_{ph}) are thermally activated with two, high and low temperature, regimes and follow the relations which can be expressed as:

$$\sigma_d = \sigma_{d1}\exp(-E_{ad1}/kT) + \sigma_{d2}(-E_{ad2}/kT) \qquad (2)$$

$$\sigma_{ph} = \sigma_{ph1}\exp(-E_{aph1}/kT) + \sigma_{ph2}(-E_{aph2}/kT) \qquad (3)$$

where T is the temperature. E_{ad1} and E_{ad2} are the activation energies for dark conductivity in the high and low temperature regimes. Similarly E_{aph1} and E_{aph2} are the activation energies for photo conductivity. Based on equations 2 and 3 we were able to simulate the conductivity responses in our samples. Henceforth we used a constant value of J_{PH} and equation 1 to predict the V_{oc} values. This is shown in Figure S7.

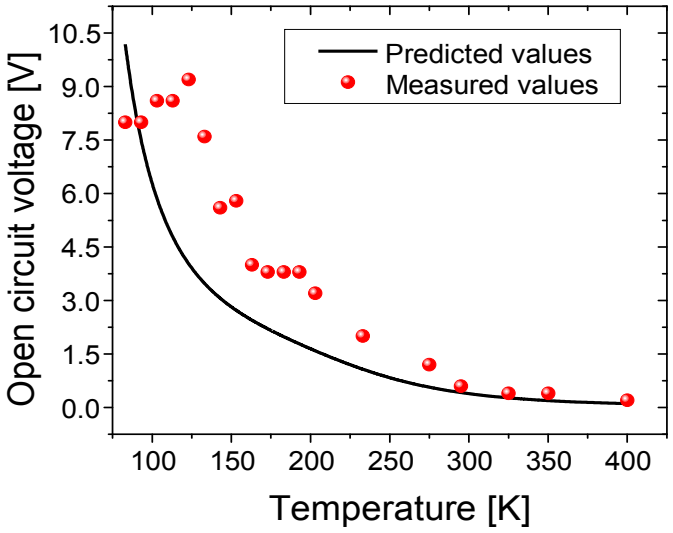

Supplementary Figure S7. Measured and predicted values of V_{oc} for a sample with 71° domains measured in PPDW geometry.

Supplementary References

[29] Ihlefeld, J. F. *et al.* Optical band gap of $BiFeO_3$ grown by molecular-beam epitaxy. *Applied Physics Letters* **92**, 142908 (2008).